DOI: 10.1002/asia.200700321

Hexagonal-Shaped Tin Glycolate Particles: A Preliminary Study of Their Suitability as Li-Ion Insertion Electrodes

See-How Ng,*[a] Sau-Yen Chew,[a] Dayse I. dos Santos,[b] Jun Chen,[c] Jia-Zhao Wang,[a] Shi-Xue Dou,[a] and Hua-Kun Liu[a]

Abstract: Tin glycolate particles were prepared by a simple, one-step, polyol-mediated synthesis in air in which tin oxalate precursor was added to ethylene glycol and heated at reflux. Hexagonal-shaped, micron-sized tin glycolate particles were formed when the solution had cooled. A series of tin oxides was produced by calcination of the synthesized tin glycolate at 600–800 °C. It was revealed that the micron-sized, hexagonal-shaped tin glycolate now consisted of nanosized tin-based particles (80–120 nm), encapsulated within a tin glycolate shell. XRD, TGA, and FT-IR measurements were conducted to account for the three-dimensional growth of the tin glycolate particles. When applied as an anode material for Li-ion batteries, the synthesized tin glycolate particles showed good electrochemical reactivity in Li-ion insertion/deinsertion, retaining a specific capacity of 416 mAh g^{-1} beyond 50 cycles. This performance was significantly better than those of all the other tin oxides nanoparticles (< 160 mAh g^{-1}) obtained after heat treatment in air. We strongly believe that the buffering of the volume expansion by the glycolate upon Li–Sn alloying is the main factor for the improved cycling of the electrode.

Keywords: electrochemistry · lithium · nanoparticles · tin glycolate

Introduction

Technological improvements in rechargeable solid-state lithium ion batteries are being driven by an ever-increasing demand for portable electronic devices and the enormous interest in the hybrid-electric-vehicle market.[1] The search for materials that provide higher storage capacity, longer operating times, and faster recharging times, as well as safety, environmental compatibility, and low production costs for a large variety of applications is a challenging task today. This has become a continuous driving force behind the search for alternative anode materials to both lithium and lithiated graphite that have capacities much higher than that of lithiated graphite (372 mAh g^{-1}),[2] but also acceptable safety features (i.e., much better than metallic lithium).

Lithium alloys, which can be reversibly formed and decomposed electrochemically in non-aqueous electrolyte solutions, are natural alternative candidates to Li anodes in rechargeable Li batteries. Indeed, there are many reports on binary and ternary Li alloys that have been tested as Li battery anodes.[3–5] Of special importance in this respect are the Li–Sn compounds, because lithium can be inserted into tin to form alloys of high Li content up to $Li_{17}Sn_4$, corresponding to a theoretical capacity of 790 mAh g^{-1}.[6] It appears that the insertion of lithium in many alloys, including Li–Sn compounds, is accompanied by pronounced volume changes (> 300 %). This leads to an intrinsic instability of the lithiated alloys in solutions: cracking, loss of passivation, intensive reduction of solution species by surface of the lithiated alloy, and electrical disconnection of active mass owing to the formation of surface films.[7] In recent years, it has been

[a] Dr. S.-H. Ng,[+] S.-Y. Chew, Dr. J.-Z. Wang, Prof. S.-X. Dou, Prof. H.-K. Liu
Institute for Superconducting & Electronic Materials
and ARC Centre of Excellence for Electromaterials Science
University of Wollongong
NSW 2522 (Australia)
Fax: (+41) 56 310 4415
E-mail: see-how.ng@psi.ch

[b] Prof. Dr. D. I. dos Santos
UNESP
São Paulo State University
CP 473 Bauru, São Paulo, (Brazil)

[c] Dr. J. Chen
Intelligent Polymer Research Institute
and ARC Centre of Excellence for Electromaterials Science
University of Wollongong,
NSW 2522 (Australia)

[+] Present address: Electrochemistry Laboratory
Paul Scherrer Institut
CH-5232 Villigen PSI, Aargau (Switzerland)

suggested that tin oxides (SnO, SnO_2) could be used as precursors for Li–Sn alloys. The lithiated tin alloys are formed while embedded in a Li_2O matrix.[8–10] Although the use of tin oxides as precursors clearly adds a considerable irreversible capacity, required for the formation of Li_2O, the formation of Li–SnO matrices seems to stabilize the repeated formation of the lithiated alloys.[11,12] It was also found that as the active mass of these systems is comprised of smaller particles, they perform better as anode materials for rechargeable batteries in terms of stability during discharge–charge (lithiation–delithiation) cycling.[13] Large absolute volume changes can be avoided when the metallic host particles are kept small. In this case, even a large volume expansion of the particles does not lead to their cracking, as the absolute changes in their dimensions are small enough.

The morphological control of thermodynamically stable SnO_2 has been widely studied, and many forms of SnO_2, such as tubes,[14] rods,[15] spheres,[16] and plates,[17] have been prepared by chemical vapour deposition[14,18] as well as by sol–gel,[19] hydrothermal,[20,21] and non-aqueous methods.[22,23] Previously, our group demonstrated the possibility of fabricating SnO_2 nanoparticles by spray pyrolysis[24] and also SnO_2 nanowires by a self-catalyzed ball-milling process.[25] Recently, we also successfully synthesized ultrafine (<5 nm) SnO_2 nanoparticles by a polyol-mediated synthesis.[26] Although the ultrafine SnO_2 nanoparticles exhibited good cyclability, retaining 400 $mAh\,g^{-1}$ after 100 cycles, the extremely high first cycle irreversible capacity loss of 72% would hamper the practical use of this material. The high irreversible capacity loss was mainly due to the high specific surface area of the nanoparticles, which resulted in an increase in surface-decomposition products with the electrolyte. Therefore, nanosized tin oxide particles will have to be protected from direct contact with the electrolyte, which was the main motivation for our study described herein.

Ethylene glycol has been widely used in the so-called polyol synthesis of metal (both pure and alloyed) nanoparticles owing to its strong reducing power and relatively high boiling point (~197 °C).[27] Owing to the high temperatures that can be applied (>150 °C), highly crystalline oxides are often obtained. Moreover, the synthesis is easy to perform and can be scaled up accordingly. Recently, Xia and co-workers successfully synthesized SnO_2 nanowires by means of a polyol-mediated synthesis, followed by calcination in air, from tin oxalate precursor and poly(vinylpyrrolidinone) (PVP) as the growth-directing agent.[28,29] Meanwhile, Ozin and co-workers also suggested the use of tin alkoxide precursors for the synthesis of self-assembled, micro-structured tin oxide materials.[30]

Herein, we report for the first time the mass synthesis of hexagonal-shaped and micro-sized tin glycolate particles through a one-step, polyol-mediated process in air from a tin oxalate precursor. The synthesized tin glycolate particles were also further calcined in air for 2 h at 600–800 °C to produce a series of tin oxides for comparison purposes. All these materials were characterized electrochemically as anode materials for Li-ion batteries. To the best of our knowledge, there is no report so far of the mass synthesis of any hexagonal-shaped organo-tin structure based on the polyol method or of its Li-ion storage capability.

Results and Discussion

The phase and purity of the powder samples were determined by X-ray diffraction (XRD), and the diffraction patterns are shown in Figure 1. Figure 1 reveals products comprising tin glycolate crystallites (Figure 1a) and nanocrystalline SnO_2 (Figure 1b–d). For the synthesized tin glycolate particles, the emergence of diffraction peaks at low angles (<20°) were characteristic of the glycolate compounds.[28–30] These peaks were attributed to the packing of building blocks associated with the glycolate polymer structure. Meanwhile, all the other patterns for the calcined samples could be readily indexed to the tetragonal phase of SnO_2 (JCPDS Card No. 41-1445), with lattice constants of $a=4.738$ Å and $c=3.187$ Å, which were found to match well with the standard XRD pattern (Figure 1e). However, tin glycolate powders that were calcined in air for 2 h at 600 °C (Figure 1b) and 700 °C (Figure 1c) also show peaks corresponding to the orthorhombic phase of SnO_2 (JCPDS Card No. 29-1484). As the calcination temperature increases (from Figure 1b to d), the intensity of the tetragonal SnO_2 phase increases significantly, whereas the intensity of the orthorhombic SnO_2 phase decreases. Tin glycolate powders calcined in air for 2 h at 800 °C (Figure 1d) revealed only peaks corresponding to the tetragonal SnO_2 phase, with no impurities detected. The well-known Debye–Scherrer formula was used to estimate the approximate average crystal size for the tin oxides using crystalline silicon as the refer-

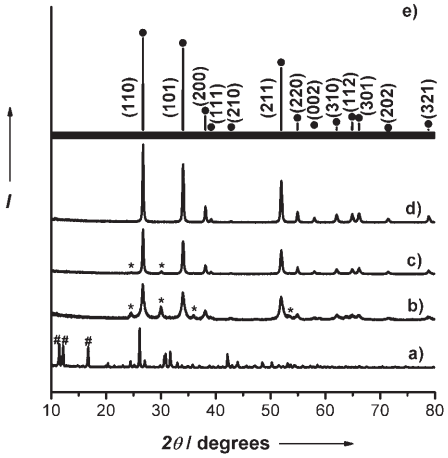

Figure 1. XRD patterns of the obtained samples: a) synthesized tin glycolate, b) tin glycolate after undergoing calcination at 600 °C for 2 h in air, c) tin glycolate after undergoing calcination at 700 °C for 2 h in air, d) tin glycolate after undergoing calcination at 800 °C for 2 h in air, and e) the standard JCPDS for SnO2 (No. 41–1445). * = orthorhombic SnO_2, # = glycolate compounds.

ence material. On the basis of the diffraction peak (110), the estimated average crystal size increased from 28 to 120 nm when the temperature increased from 600 to 800 °C.

The compositional and structural changes associated with the calcination process were also monitored by thermogravimetric analysis (TGA) and Fourier transform infrared (FT-IR) spectroscopy methods. Figure 2a shows the TGA curve

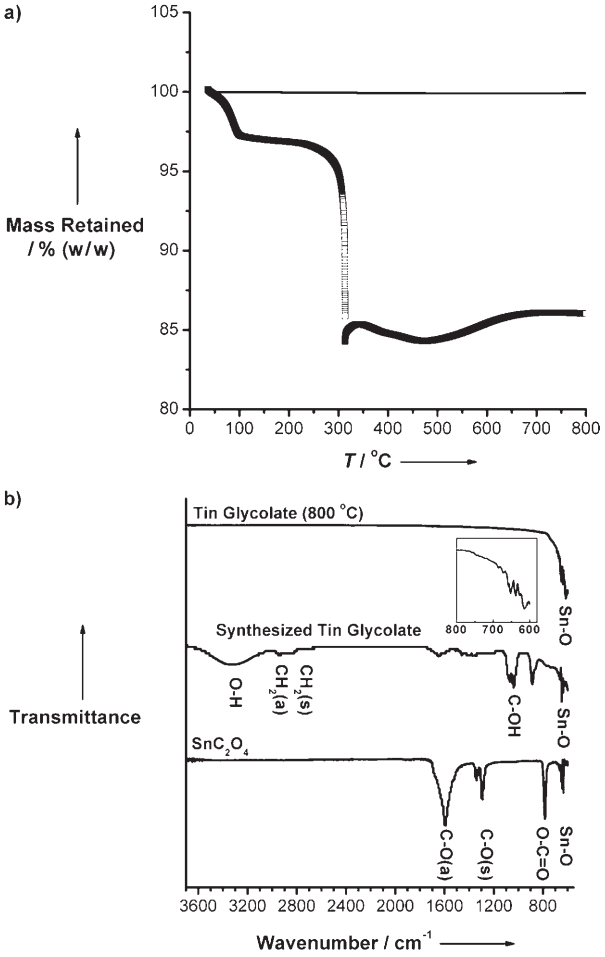

Figure 2. a) TGA curves of the synthesized tin glycolate (□) and the tin glycolate after calcination at 800 °C for 2 h in air (solid line), and b) FT-IR spectra for the tin oxalate precursor powder, the synthesized tin glycolate, and the tin glycolate after undergoing calcination at 800 °C for 2 h in air. For the sample calcined at 800 °C, a magnified view (inset) of the region corresponding to the Sn–O stretching band is also given.

recorded under a flow of oxygen gas, indicating a two-step pattern for weight loss in the temperature ranges of 25 to 100 °C and 250 to 320 °C, respectively. The first weight loss could be attributed to the desorption of physically adsorbed water and ethylene glycol molecules, and the second could be ascribed to the removal of ethylene glycol units chemically bonded to the tin element in the glycolate crystals.[28–30] Typically, we observed a weight loss of ~3.0% for the first step and ~13.0% for the second step. Furthermore, the mass increased at temperatures above 500 °C and reached a steady mass at temperatures above 700 °C. This was due to the complete oxidation of residual SnO_x (for example SnO and Sn_3O_4) to SnO_2. This is a very common feature for Sn-based oxide materials.[28–30] Finally, the calcined sample did not show any weight loss for the temperature range up to 800 °C. This confirms that the calcined sample consists of only SnO_2 crystallites.

Figure 2b shows FT-IR spectra recorded from the tin oxalate precursor powder, the synthesized tin glycolate particles, and also from the calcined sample at 800 °C. After the polyol-mediated process, the O–C=O vibrational bands from the oxalate group at ~785 cm^{-1} disappeared, whereas bands for the CH_2 and C–OH groups from the ethylene glycol unit at ~2900 cm^{-1} and ~1050 cm^{-1}, respectively, were present. The peaks corresponding to physically absorbed water or ethylene glycol units (the O–H stretching mode at ~3310 cm^{-1} and the C–OH bending mode at ~1050 cm^{-1}) disappeared after calcination at 800 °C in air for 2 h. At this temperature, only the Sn–O stretching band still remained at ~610 cm^{-1}, indicating the formation of nanocrystalline SnO_2.[31–33] These observations were consistent with previous studies in which conventional alkoxides were used as sol–gel precursors to prepare various phases of tin oxides.[30]

Scanning electron microscopy (SEM) images of the synthesized tin glycolate particles and the corresponding calcined products, tin oxide particles, are shown in Figure 3. As can be seen from Figure 3a, the synthesized tin glycolate

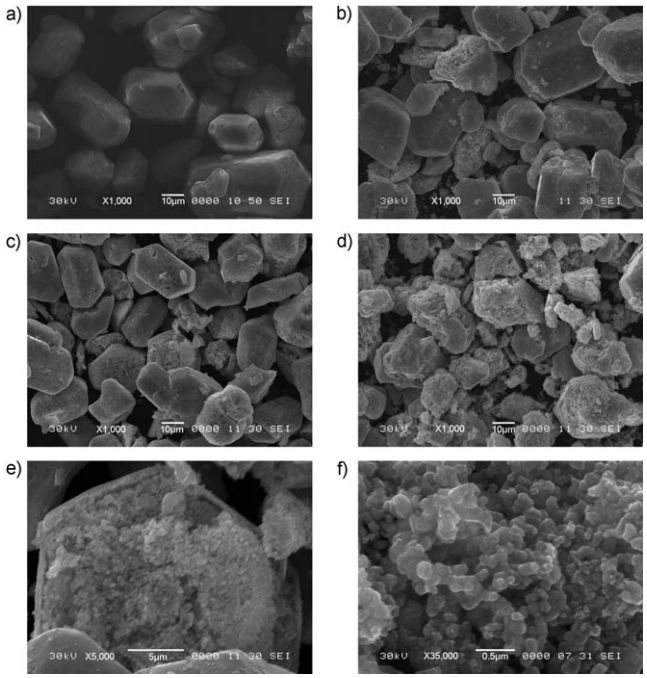

Figure 3. SEM images of the obtained samples: a) synthesized tin glycolate, b) tin glycolate after undergoing calcination at 600 °C for 2 h in air, c) tin glycolate after undergoing calcination at 700 °C for 2 h in air, d) tin glycolate after undergoing calcination at 800 °C for 2 h in air, e) corresponding higher magnification image of c) revealing encapsulation of tin oxide nanoparticles inside the hexagonal-shaped tin glycolate shell, and f) corresponding higher magnification image of e) confirming the nanosize nature of the tin oxide particles.

particles have hexagonal-shaped microstructures, with particle sizes up to 50 μm. However, after the synthesized tin glycolate powders were calcined in air for 2 h at 600–800 °C (Figure 3 b–d), the hexagonal-shaped microstructures were destroyed, revealing nanosized particles encapsulated within hexagonal-shaped glycolate shells (Figure 3 e). The extent of the destruction of the encapsulation becomes worse when the calcination temperature increases from 600 to 800 °C. The average particle sizes observed in Figure 3 f were between 80–120 nm, which matches well with the prediction from XRD measurements earlier (see Figure 1).

The closely packed nature of the nanoparticles supports the formation of a two-dimensional aggregation of the nanoparticles into hexagonal-shaped tin glycolate microstructures, as illustrated in Figure 4. At the initial stage of refluxing, the oxalate groups from SnC_2O_4 were replaced with ethylene glycol units, which is also supported by FT-IR measurements (Figure 2 b) with the appearance of bands for CH_2 and C−OH and the disappearance of the O−C=O vibrational bands.[31–33] Further refluxing results in further reactions of tin glycolate and eventually relatively large polymer-like particles are formed, which are then self-assembled into hexagonal-shaped microstructures through a two-dimensional aggregation of the nanostructures. The key step is the polymerization of tin glycolate, a process that has been discussed in a number of publications for the same or similar metal alkoxides.[28–30]

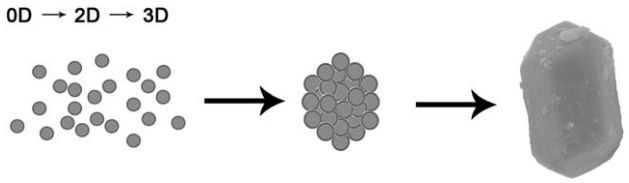

Figure 4. A plausible organizing scheme for the self-construction of complex geometrical structures (e.g., polyhedra) by oriented attachment of nanostructures.

The electrochemical Li-storage properties of the synthesized tin glycolate and the corresponding calcined products, tin oxide nanoparticles, were systematically investigated. Generally, SnO_2 reacts with lithium in a two-step process,[3–13,16,24–26] as follows [Eq. (1)] and [Eq. (2)]:

$$SnO_2 + 4Li^+ + 4e^- \rightarrow Sn + 2Li_2O \quad (1)$$

$$Sn + xLi^+ + xe^- \leftrightarrow Li_xSn, (0 \le x \le 4.4) \quad (2)$$

The first process is an irreversible reaction [Eq. (1)] in which SnO_2 is reduced to tin with the formation of a Li_2O matrix. This reaction normally occurs at a potential below 0.9 V vs. Li/Li^+.[26] This reaction could contribute an irreversible capacity as high as 710 mAh g^{-1}. Meanwhile, the second reaction [Eq. (2)] corresponds to the reversible formation of Li_xSn alloys ($0 \le x \le 4.4$). The theoretical reversible capacity from this reaction is 790 mAh g^{-1}. The Li–Sn alloying process normally occurs at a potential below 0.6 V.[26] Therefore, the total discharge capacity for the first cycle could be as high as 1500 mAh g^{-1}.

Cyclic voltammograms (CVs) in the potential range of 0.01–1.50 V vs. Li/Li^+ were used to analyze the electrochemical Li-ion insertion properties of all the obtained samples (Figure 5). As can be seen from all the CVs, a strong and broad cathodic peak occurred at potentials above 0.6 V, which corresponds to the formation of Sn metal in a Li_2O matrix. However, each sample exhibited a different potential region for this reaction. There is a distinct contrast between the synthesized tin glycolate electrode (Figure 5 a) and the other calcined products, tin oxide electrodes (Figure 5 b–d). The higher reduction peak (~1.2 V vs. Li/Li^+) observed for the synthesized tin glycolate electrode was due to the lower valence state (+2) of the tin element in the compound, and also the contribution from the glycolate part in the surface film formation process.[6,11–12,31] Meanwhile, the calcined products, tin oxide electrodes, gave a broad cathodic peak at 0.8 V vs. Li/Li^+. Moreover, tin glycolate samples calcined in air at 600 °C (Figure 5 b) and 700 °C (Figure 5 c) also show a small cathodic peak at 0.68 V, which was due to traces of orthorhombic SnO_2, as confirmed by the XRD measurements in Figure 1. Further cycling led to well-defined and almost identical reduction and oxidation peaks at 0.2 and 0.5 V vs. Li/Li^+ for all the electrodes. Furthermore, the cycling kinetics for the synthesized tin glycolate electrode seems to be fairly stable over the first 10 cycles, whereas the calcined products, the tin oxide electrodes, suffer rapid decay in the redox kinetics.

Figure 6 summarizes the 1st, 2nd, 10th, 20th, and 50th electrochemical lithiation (discharge)/delithiation (charge) capacity data for the synthesized tin glycolate electrode (Figure 6 a) and the calcined samples, that is, the tin oxide electrodes (Figure 6 b–d). The calculated capacities were based solely on the active materials, either tin glycolate or tin oxide particles in the electrodes. The first cycle discharge capacities were 1541, 1441, 1223, and 1377 mAh g^{-1} for the synthesized tin glycolate electrodes and the electrodes of tin glycolate powders calcined in air at 600, 700, and 800 °C, respectively, with the corresponding first cycle charge capacities 832, 741, 742, and 738 mAh g^{-1}. Therefore, the first cycle couloumbic efficiencies were 54 %, 51 %, 61 %, and 54 % for the synthesized tin glycolate electrode and the electrodes of tin glycolate powders calcined in air at 600, 700, and 800 °C, respectively. The large irreversible capacity loss could be attributed to the formation of Li_2O and also to irreversible trapping of lithium by the solid electrolyte interface (SEI) passivation layer. All electrodes show capacity fading behavior upon prolonged cycling. However, the synthesized tin glycolate electrode still maintained fairly high Li-ion insertion/deinsertion capacities, even after 50 cycles, relative to the other tin oxide electrodes.

Figure 7 shows the cycling behavior of the synthesized tin glycolate electrode and the corresponding calcined samples, the tin oxide electrodes. When using a nonrestricted cycling procedure, on cycling between 0.01 and 1.50 V vs. Li/Li^+ at

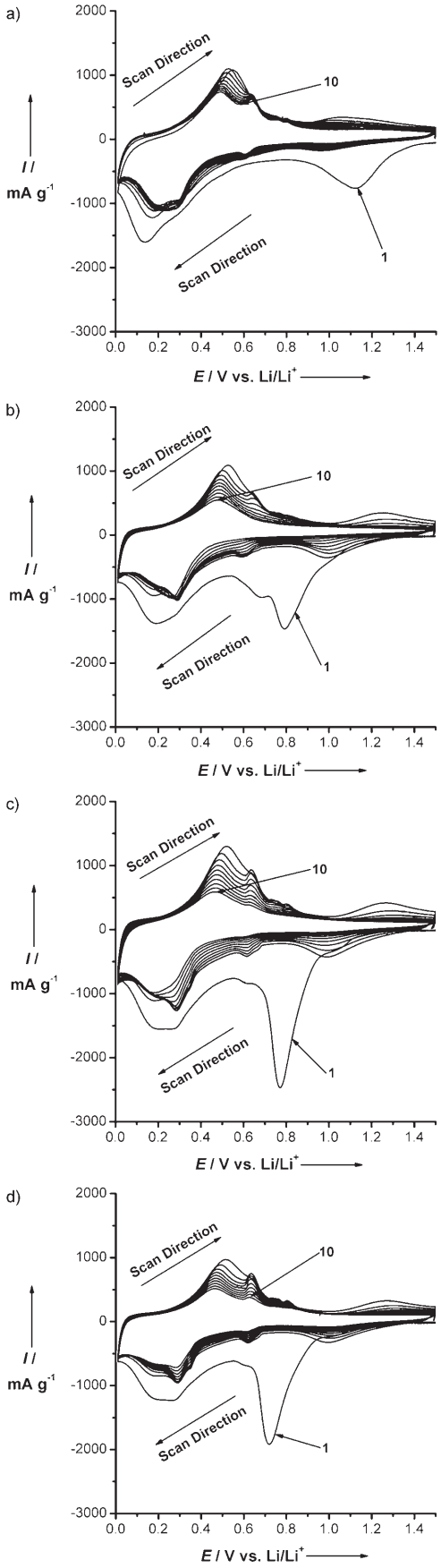

Figure 5. Cyclic voltammograms in the first 10 cycles for all the obtained samples: a) synthesized tin glycolate, b) tin glycolate after undergoing calcination at 600 °C for 2 h in air, c) tin glycolate after undergoing calcination at 700 °C for 2 h in air, and d) tin glycolate after undergoing calcination at 800 °C for 2 h in air (with the numbers indicating the cycle number). Cycling took place between 0.01 and 1.50 V vs. Li/Li^+ at a scan rate of 0.1 $mV s^{-1}$. I = current density, E = cell potential.

a cycling rate of 50 $mA g^{-1}$, the initial reversible capacities (2nd discharge capacity) were 934, 758, 758, and 756 $mAh g^{-1}$ for the electrodes composed of the synthesized tin glycolate and of tin glycolate powders calcined in air at 600, 700, and 800 °C, respectively. Subsequently, the reversible capacities beyond 50 cycles were maintained at 416, 155, 90, and 108 $mAh g^{-1}$ for the as-synthesized tin glycolate electrode and the electrodes of tin glycolate powders calcined in air at 600, 700, and 800 °C, respectively, corresponding to the ratios of the specific capacities retained after 50 cycles to the first discharge capacities, which are 44 %, 20 %, 12 %, and 14 %, respectively. The superior capacity retention of the synthesized tin glycolate electrode over that of the other tin oxide electrodes suggests the beneficial effect of the encapsulation by the glycolate microstructures in buffering the volume expansion during the alloying reactions.

Figure 8 shows the cycling behavior of the synthesized tin glycolate electrode, which was cycled between 0.01 and 1.50 V vs. Li/Li^+ at a cycling rate of 50 $mA g^{-1}$. The synthesized tin glycolate electrode shows moderate capacity fading in the first 20 cycles, followed by a relatively flat and low capacity fading for the next 30 cycles. The synthesized tin glycolate electrode shows an irreversible capacity loss (Q_{irrev}) of less than 1.2 % per cycle. However, the discharge capacities for the first ten cycles (> 800 $mAh g^{-1}$) were far beyond our expectation. SnO_2 has a theoretical specific reversible capacity of 790 $mAh g^{-1}$. According to the thermogravimetric analysis (TGA) results shown earlier in Figure 2 a, SnO_2 was 84 % (w/w) in the tin glycolate compound. This means that the specific capacity from SnO_2 should not exceed 664 $mAh g^{-1}$. Where do the excess capacities come from?

It has been reported in the literature that transition metal oxides show reversible Li-storage behaviour.[34] In those cases, a transition metal can react with Li_2O upon Li extraction. This means that the reaction in [Eq. (1)] is reversible, which contributes to a very high reversible capacity. Up to now, no experimental evidence has shown whether the reaction in [Eq. (1)] for Sn-based oxides is completely irreversible or not. However, Courtney et al. reported that Li–O bonds are not stable when the charging voltage is above 1.3 V.[35] Recently, Li et al. also indicated that the reaction in [Eq. (1)] is reversible for most metal compounds in view of their thermodynamic properties. The reversibility of the reaction in [Eq. (1)] from LiX (e.g., Li_2O) and metal (e.g., Sn) back to metal compounds is mainly influenced by the intrinsic conductivity of the MX compound, the grain size of the LiX and the metal, the separation distance between LiX and the metal, and the electronic contact with the conductive additive.[36] For the synthesized tin glycolate microstruc-

CHEMISTRY
AN ASIAN JOURNAL

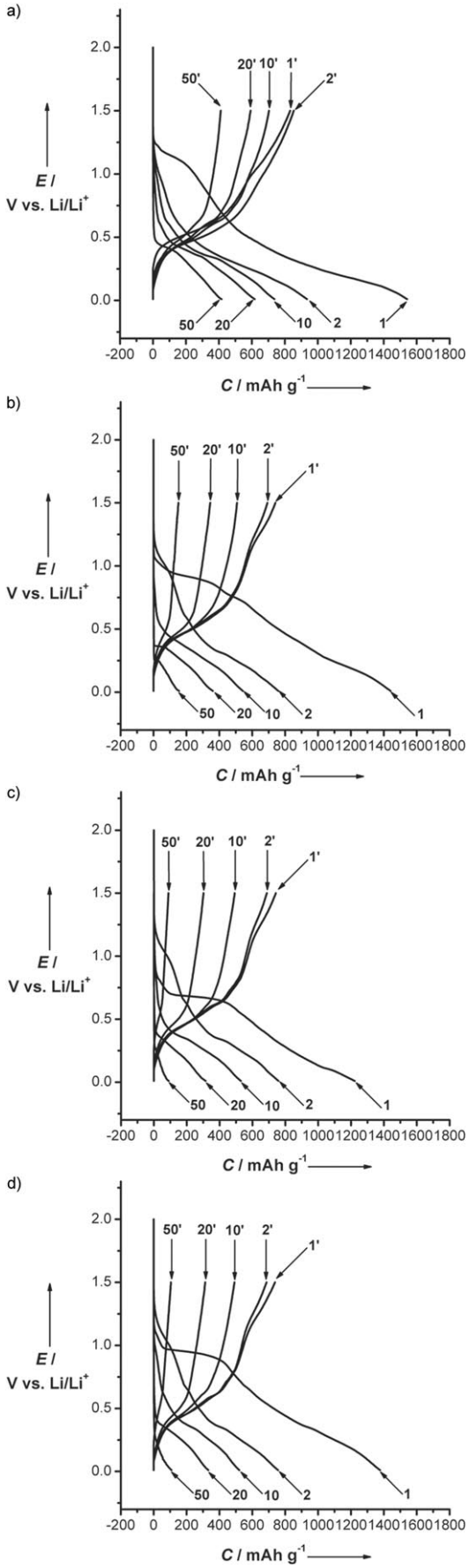

Figure 6. Charge–discharge profiles of all the obtained samples: a) synthesized tin glycolate, b) tin glycolate after undergoing calcination at 600 °C for 2 h in air, c) tin glycolate after undergoing calcination at 700 °C for 2 h in air, and d) tin glycolate after undergoing calcination at 800 °C for 2 h in air (with the numbers indicating the cycle number). Cycling took place between 0.01 V and 1.50 V vs. Li/Li^+ at a cycling rate of 50 mA g^{-1}. C = capacity, E = cell potential.

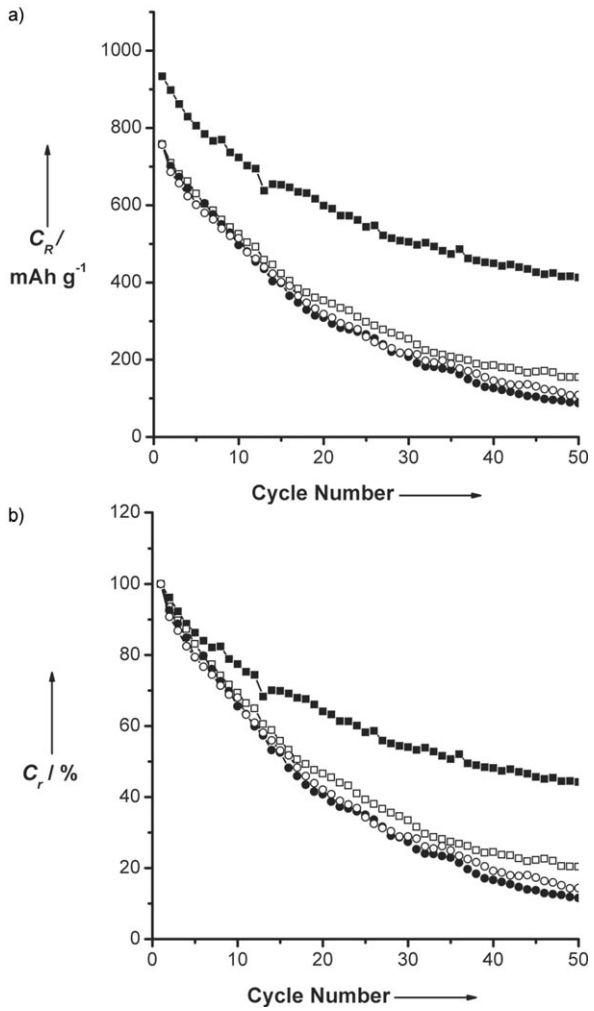

Figure 7. Cycling behavior of electrodes for all the obtained samples (-■- synthesized tin glycolate; -□- tin glycolate after undergoing calcination at 600 °C for 2 h in air; -●- tin glycolate after undergoing calcination at 700 °C for 2 h in air; and -○- in glycolate after undergoing calcination at 800 °C for 2 h in air): a) reversible capacities as a function of cycle number, and b) the corresponding percentage of reversible capacity retained as a function of cycle number. Cycling took place between 0.01 V and 1.50 V vs. Li/Li^+ at a cycling rate of 50 mA g^{-1}. C_R = reversible capacity, C_r = retained capacity.

tures, the Sn-based nanoparticles are embedded in a glycolate capsule, which ensures that the Li_2O and Sn element formed are in good contact, without any distinct separation. This provides a kinetic advantage for the reversible reaction in [Eq. (1)]. We believe that the reaction in [Eq. (1)] is at least partially reversible for the first few cycles (in our case), which contributes to the unusually high reversible capacity.

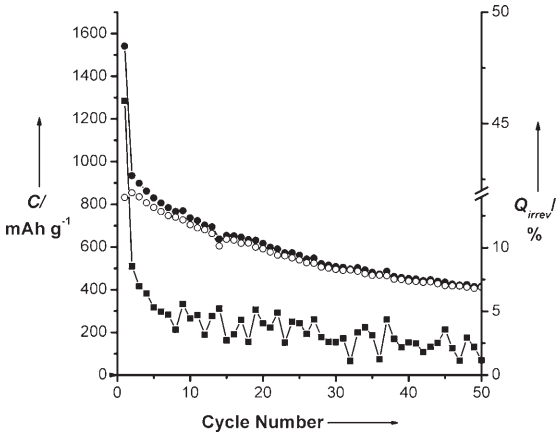

Figure 8. Cycling behavior for an electrode made from the synthesized tin glycolate. Cycling took place between 0.01 V and 1.50 V vs. Li/Li^+ at a cycling rate of 50 mA g^{-1}. -●-=Li^+ insertion, -○-=Li^+ extraction, C=specific capacity, Q_{irrev}%=percentage of irreversible capacity loss.

The morphologies of the electrodes after prolonged cycling were examined by scanning electron microscopy (SEM). Figure 9 shows SEM images for the synthesized tin

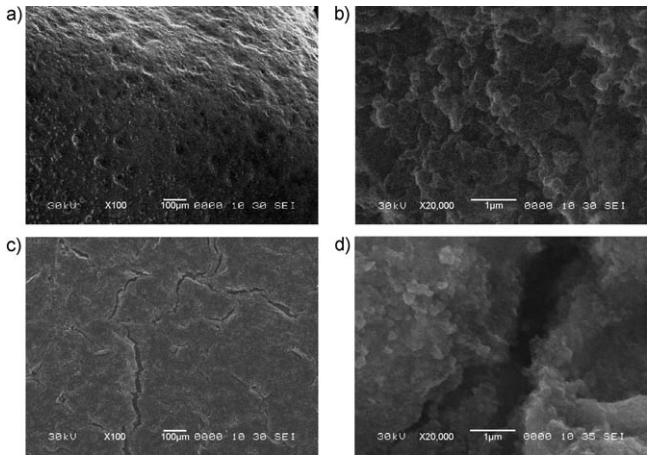

Figure 9. SEM images of the electrodes after 50 cycles for the synthesized tin glycolate: a) low-magnification image and b) the corresponding high-magnification image; and for tin glycolate after undergoing calcination at 800 °C for 2 h in air: c) low-magnification image and d) the corresponding high-magnification image.

glycolate electrode (Figure 9a,b) and the electrode composed of tin glycolate powder calcined in air for 2 h at 800 °C (Figure 9c,d) after 50 electrochemical lithiation/delithiation cycles. Huge cracks were observed in the calcined sample, with the crack width estimated to be approximately 3 μm. The reason for the creation of the cracks is the pronounced changes in the volume of the host material under alloying/dealloying processes.[31] These cracking phenomena upon cycling indicate problems associated with the integrity of the active mass. Cracking causes obvious problems related to the passivation of these electrodes by stable surface films. It is very likely that part of the active mass becomes isolated by surface films formed on the fresh active surface that the cracks expose, by reactions of Li–Sn compounds and solution components. Thereby, the capacity of the electrodes fades rapidly during cycling. Meanwhile, the synthesized tin glycolate microstructured electrode still maintained the integrity and good contacts between the Sn-based nanoparticles after Li-ion insertion. This proves that the encapsulation of the Sn-based nanoparticles in the glycolate microstructures played an important role in maintaining the integrity of the electrode upon prolonged cycling.

The cyclic performance of the synthesized tin glycolate crystals is still not satisfactory and may benefit from further optimization. Despite that, this result illustrates the good prospect that the capacity of glycolate anodes may be significantly enhanced by an optimized microstructure. Moreover, because many tin-based compounds have been demonstrated as promising high-capacity negative-electrode materials for use in lithium-ion batteries,[16,21,24–26,31] there still exists plenty of room for the improvement of tin glycolate structures with respect to their Li-storage properties. Further research is now in progress.

Conclusions

In summary, micron-sized, hexagonal-shaped tin glycolate with encapsulation of electrochemically active tin-based nanoparticles has been successfully prepared by a one-step, polyol-mediated synthesis route. The synthesis is based on the two-dimensional aggregation of the organo-tin nanocrystallites giving an overall quasi-hexagonal microstructure in the presence of ethylene glycol after continuous refluxing in air at 195 °C for 5 h. This synthetic procedure is straightforward and inexpensive, and consequently can be readily adopted to produce large quantities of uniform, hexagonal-shaped tin glycolate. Furthermore, when applied as an anode material for lithium-ion batteries, the synthesized tin glycolate exhibit promising Li-ion storage capability, retaining a specific capacity of 416 mAh g^{-1} beyond 50 cycles. The encapsulation of the electrochemically active tin-based nanoparticles in the hexagonal-shaped tin glycolate was the main reason for the improved electrochemical cycling, because they buffered volume expansion and decreased solid/electrolyte interphase formation in the electrode. Further investigations will enable us to elucidate the Li-ion-insertion mechanism and lead to a better understanding of the capacity-fading behavior of the tin glycolate electrode.

Experimental Section

Synthesis

In a typical procedure, $SnC_2O_4{\cdot}2H_2O$ (Sigma–Aldrich, 98%) (0.5 g) was added to ethylene glycol (EG, Sigma–Aldrich, anhydrous, 99.8%) (50 mL) in a round-bottomed flask and heated at reflux at 195 °C under ambient pressure. The reaction can be easily followed through its distinctive colour changes. During the following 45 min, the cloudy mixture

turned into a clear solution. After the solution had been heated at reflux under constant stirring for 5 h, a white precipitate began to appear in the light yellow solution, indicating the formation of the tin glycolate crystals. After the reaction had been stopped by cooling down the solution to room temperature, the white precipitate was collected by centrifugation at 4400 rpm, followed by washing with ethanol and acetone to remove physically adsorbed ethylene glycol. Finally, the synthesized tin glycolate powder was dried for 30 min at 80 °C in a vacuum oven. To compare the electrochemical properties of the synthesized tin glycolate crystals with standard tin oxides, a series of tin oxide powders were produced by calcining the synthesized tin glycolate crystals in air for 2 h at 600, 700, and 800 °C.

Characterization

X-ray diffraction (XRD) data were collected from powder samples on a Philips PW1730 diffractometer (with $Cu_{K\alpha}$ radiation, $\lambda = 1.54056$ Å) at a scanning rate of $2° min^{-1}$ for 2θ in the range 10–80°. Thermogravimetric analyses (TGA) were carried out on a TA Instruments Q500 (USA) at a heating rate of $10 °C min^{-1}$ under a flow of oxygen gas. Fourier-transform infrared (FT-IR) spectra were acquired under ambient conditions on a Nicolet Avatar 360 Fourier Transform Infrared Spectrophotometer with a resolution of $0.5\ cm^{-1}$. Scanning electron microscopy (SEM) images were captured on a scanning electron microscope (JEOL, JSM 6460 A) operated at an acceleration voltage of 30 kV.

Electrochemical Measurements

The anode was prepared by mixing synthesized tin glycolate crystals or calcined tin glycolate powders (at 600, 700, and 800 °C) as active materials with 20% (*w*/*w*) carbon black (Super P, Timcal, Belgium) and 10% (*w*/*w*) poly(vinylidene fluoride) (PVDF, Sigma–Aldrich) binders in *N*-methyl-2-pyrrolidinone (NMP, Sigma–Aldrich, anhydrous, 99.5%) solvent to form a homogeneous slurry, which was then spread onto a copper foil. The coated electrodes (average thickness ~50 μm) were dried in a vacuum oven at 110 °C for 24 h and then pressed. Electrochemical measurements were carried out by using coin-type cells. CR 2032 coin-type cells were assembled in an argon-filled glove box (Mbraun, Unilab, Germany) by stacking a porous polypropylene separator containing liquid electrolyte between the composite electrodes and a lithium foil counter-electrode. The electrolyte used was $LiPF_6$ (1 M) in a 50:50 (*w*/*w*) mixture of ethylene carbonate (EC) and dimethyl carbonate (DMC), provided by MERCK KgaA, Germany. The cells were galvanostatically discharged and charged in the range 0.01–1.50 V vs. Li/Li^+ at a constant current density of $50\ mA g^{-1}$ by using a Neware battery tester. Cyclic voltammetry (CV) measurements were performed at a scanning rate of $0.1\ mV s^{-1}$ on a CHI 660C electrochemical workstation system (CH Instrument, Cordova TN).

Acknowledgements

This research was supported in part by ARC Center of Excellence funding under grant number CE0561616 administered through the University of Wollongong. D. I. dos Santos thanks the National Council for Scientific and Technological Development (CNPq-Brazil) for a fellowship (No. 201126/2004–4). We thank Dr. T. Silver (University of Wollongong) for critical reading of the manuscript.

[1] J.-M. Tarascon, M. Armand, *Nature* **2001**, *414*, 359–367.
[2] S. H. Ng, J. Wang, D. Wexler, K. Konstantinov, Z. P. Guo, H. K. Liu, *Angew. Chem.* **2006**, *118*, 7050–7053; *Angew. Chem. Int. Ed.* **2006**, *45*, 6896–6899.
[3] J. R. Dahn, I. A. Courtney, O. Mao, *Solid State Ionics* **1998**, *111*, 289–294.
[4] W. Liu, X. Huang, Z. Wang, H. Li, L. Chen, *J. Electrochem. Soc.* **1998**, *145*, 59–62.
[5] M. Mohamedi, S. J. Lee, D. Takahashi, M. Nishizawa, T. Itoh, I. Uchida, *Electrochim. Acta* **2001**, *46*, 1161–1168.
[6] M. Winter, J. O. Besenhard, *Electrochim. Acta* **1999**, *45*, 31–50.
[7] R. A. Huggins, *Solid State Ionics* **1998**, *113–115*, 57–67.
[8] T. Brousse, R. Retoux, H. Herterich, D. M. Schleich, *J. Electrochem. Soc.* **1998**, *145*, 1–4.
[9] J. Chouvin, C. Branci, J. Sarradin, J. Olivier-Fourcade, J. C. Jumas, B. Simon, Ph. Biensan, *J. Power Sources* **1999**, *81–82*, 277–281.
[10] C. Wang, A. J. Appleby, F. E. Little, *J. Power Sources* **2001**, *93*, 174–185.
[11] Y. Idota, T. Kubota, A. Matsufuji, Y. Maekawa, T. Miyasaka, *Science* **1997**, *276*, 1395–1397.
[12] I. A. Courtney, J. R. Dahn, *J. Electrochem. Soc.* **1997**, *144*, 2045–2052.
[13] M. Winter, J. O. Besenhard, M. E. Spahr, P. Novak, *Adv. Mater.* **1998**, *10*, 725–763.
[14] Y. Liu, M. Liu, *Adv. Funct. Mater.* **2005**, *15*, 57–62.
[15] C. Guo, M. Cao, C. Hu, *Inorg. Chem. Commun.* **2004**, *7*, 929–931.
[16] S. Han, B. Jang, T. Kim, S. M. Oh, T. Hyeon, *Adv. Funct. Mater.* **2005**, *15*, 1845–1850.
[17] H. Ohgi, T. Maeda, E. Hosono, S. Fujihara, H. Imai, *Cryst. Growth Des.* **2005**, *5*, 1079–1083.
[18] J. Duan, S. Yang, H. Liu, J. Gong, H. Huang, X. Zhao, R. Zhang, Y. Du, *J. Am. Chem. Soc.* **2005**, *127*, 6180–6181.
[19] M. Shoyama, N. Hashimoto, *Sens. Actuators B* **2003**, *93*, 585–589.
[20] H. G. Yang, H. C. Zeng, *Angew. Chem.* **2004**, *116*, 6056–6059; *Angew. Chem. Int. Ed.* **2004**, *43*, 5930–5933.
[21] X. Sun, J. Liu, Y. Li, *Chem. Mater.* **2006**, *18*, 3486–3494.
[22] N. Pinna, G. Neri, M. Antonietti, M. Niederberger, *Angew. Chem.* **2004**, *116*, 4445–4449; *Angew. Chem. Int. Ed.* **2004**, *43*, 4345–4349.
[23] J. Ba, J. Polleux, M. Antonietti, M. Niederberger, *Adv. Mater.* **2005**, *17*, 2509–2512.
[24] L. Yuan, Z. P. Guo, K. Konstantinov, H. K. Liu, S. X. Dou, *J. Power Sources* **2006**, *159*, 345–348.
[25] M. S. Park, G. X. Wang, Y. M. Kang, D. Wexler, H. K. Liu, S. X. Dou, *Angew. Chem.* **2007**, *119*, 764–767; *Angew. Chem. Int. Ed.* **2007**, *46*, 750–753.
[26] S. H. Ng, D. I. dos Santos, S. Y. Chew, D. Wexler, J. Wang, S. X. Dou, H. K. Liu, *Electrochem. Commun.* **2007**, *9*, 915–919.
[27] C. Feldmann, *Adv. Funct. Mater.* **2003**, *13*, 101–107.
[28] Y. Wang, X. Jiang, Y. Xia, *J. Am. Chem. Soc.* **2003**, *125*, 16176–16177.
[29] X. Jiang, Y. Wang, T. Herricks, Y. Xia, *J. Mater. Chem.* **2004**, *14*, 695–703.
[30] R. W. J. Scott, N. Coombs, G. A. Ozin, *J. Mater. Chem.* **2003**, *13*, 969–974.
[31] J. Zhu, Z. Lu, S. T. Aruna, D. Aurbach, A. Gedanken, *Chem. Mater.* **2000**, *12*, 2557–2566.
[32] D. Aurbach, A. Nimberger, B. Markovsky, E. Levi, E. Sominski, A. Gedanken, *Chem. Mater.* **2002**, *14*, 4155–4163.
[33] Q. Zhao, Z. Zhao, T. Dong, Y. Xie, *J. Phys. Chem. B* **2006**, *110*, 15152–15156.
[34] P. Poizot, S. Laruelle, S. Grugeon, L. Dupont, J. M. Tarascon, *Nature* **2000**, *407*, 496–499.
[35] I. A. Courtney, J. R. Dahn, *J. Electrochem. Soc.* **1997**, *144*, 2943–2948.
[36] H. Li, P. Balaya, J. Maier, *J. Electrochem. Soc.* **2004**, *151*, A1878–A1885.

Received: September 5, 2007
Published online: March 26, 2008

